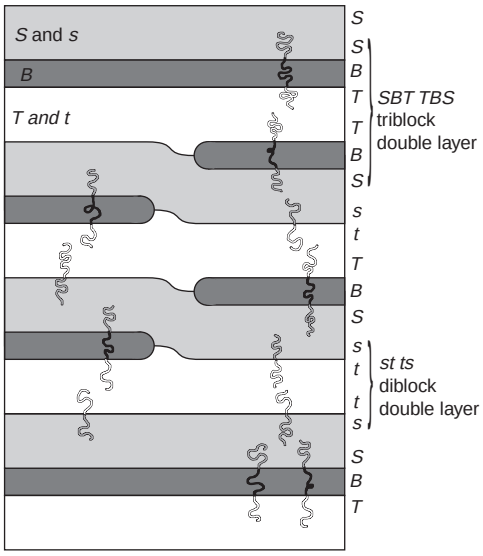

Figure 3 Chain orientations at a morphological defect of a lamellar non-centrosymmetric blend of SBT and st block copolymers.

poly(methyl methacrylate) and polybutadiene-block-poly(methyl methacrylate) (not shown).

The results that we report here have shown that non-centrosymmetric materials may be produced by amorphous self-assembling block copolymer blends. By changing the molecular weights of the blend components, control of the periodic length should be possible: this concept should make accessible periodic non-centrosymmetric materials with a well defined long-range periodicity that is within the mesoscopic length scale. Other monomers might be considered for introducing useful molecular properties into such a non-centrosymmetric material. □

Methods

Synthesis. Block copolymers were synthesized by sequential anionic polymerization of different monomers. A polystyrene-block-polybutadiene-block-poly(*tert*-butyl methacrylate) triblock copolymer (SBT) and a polystyrene-block-poly(*tert*-butyl methacrylate) diblock copolymer (st) were synthesized in tetrahydrofuran in the presence of lithium alkoxides using *sec*-butyllithium as initiator. Details are given in ref. 22; TBMA is treated as MMA except for the polymerization temperature, which is increased over 2 h from −60 °C to −40 °C. The characteristics of the block copolymers are given in Table 1.

Sample preparation. The blend components were dissolved together in chloroform which was evaporated over several weeks. For further equilibration, the dry films were annealed at 150 °C for 6 h in vacuum.

Transmission electron microscopy. This was performed using a ZEISS 902 transmission electron microscope operating at 80 kV in the bright-field mode. Ultrathin sections of the samples were obtained using a Reichert ultra-microtome equipped with a diamond knife.

Small angle X-ray scattering. This was performed using a Bruker AXS 2D-SAXS Nanostar instrument, operating with Cu Kα radiation, at the Application Laboratory of A. Paar KG in Graz, Austria.

Received 2 November 1998; accepted 19 January 1999.

1. Landau, L. D. & Lifshitz, E. M. *Electrodynamics of Continuous Media* 2nd edn (Pergamon, Oxford, 1987).
2. Nye, J. F. *Physical Properties of Crystals* (Oxford Univ. Press, New York, 1960).
3. Yariv, A. *Quantum Electronics* 64 (Saunders College Publishing, Philadelphia, 1991).
4. Bates, F. S. & Fredrickson, G. H. Block copolymer thermodynamics: theory and experiment. *Annu. Rev. Phys. Chem.* **41,** 525–557 (1990).
5. Binder, K. Phase transitions in polymer blends and block copolymer melts: some recent developments. *Adv. Polym. Sci.* **112,** 181–299 (1994).
6. de Gennes, P. G. *The Physics of Liquid Crystals* (Oxford Univ. Press, 1973).
7. Jacobs, A. E., Goldner, G. & Mukamel, D. Modulated structures in tilted chiral smectic films. *Phys. Rev. A* **45,** 5783–5788 (1992).
8. Petschek, R. G. & Wiefling, K. M. Novel ferroelectric fluids. *Phys. Rev. Lett.* **59,** 343–346 (1987).
9. Halperin, A. Rod-coil copolymers: their aggregation behavior. *Macromolecules* **23,** 2724–2731 (1990).
10. Prost, J., Bruinsma, R. & Tournilhac, F. Theory of longitudinal ferroelectric smectics. *J. Phys. II France* **4,** 169–187 (1994).
11. Tournilhac, F., Blinov, L. M., Simon, J. & Yablonsky, S. V. Ferroelectric liquid crystals from achiral molecules. *Nature* **359,** 621–623 (1992).
12. Stupp, S. I. *et al.* Supramolecular materials: self-organized nanostructures. *Science* **276,** 384–389 (1997).
13. Niori, T., Sekine, T., Watanabe, J., Furukawa, T. & Takezone, H. Distinct ferroelectric smectic liquid crystals consisting of banana shaped achiral molecules. *J. Mater. Chem.* **6,** 1231–1233 (1996).
14. Link, D. R. *et al.* Spontaneous formation of macroscopic chiral domains in a fluid smectic phase of achiral molecules. *Science* **278,** 1924–1927 (1997).
15. Mogi, Y. *et al.* Molecular weight dependence of the lamellar domain spacing of ABC triblock copolymers and their chain conformations in lamellar domains. *Macromolecules* **26,** 5169–5173 (1993).
16. Gido, S. P., Schwark, D. W., Thomas, E. L. & Goncalves, M. C. Observation of a non-constant mean curvature interface in an ABC triblock copolymer. *Macromolecules* **26,** 2636–2640 (1993).
17. Stadler, R. *et al.* Morphology and thermodynamics of symmetric poly(A-block-B-block-C) triblock copolymers. *Macromolecules* **28,** 3080–3097 (1995).
18. Breiner, U., Krappe, U. & Stadler, R. Evolution of the "knitting pattern" morphology in ABC triblock copolymers. *Macromol. Rapid Commun.* **17,** 567–575 (1996).
19. Breiner, U., Krappe, U., Abetz, V. & Stadler, R. Cylindrical morphologies in asymmetric ABC triblock copolymers. *Macromol. Chem. Phys.* **198,** 1051–1083 (1997).
20. Brinkmann, S., Stadler, R. & Thomas, E. L. New structural motif in hexagonally ordered cylindrical ternary (ABC) block copolymer domains. *Macromolecules* **31,** 6566–6572 (1998).
21. Krappe, U., Stadler, R. & Voigt-Martin, I.-G. Chiral assembly in amorphous ABC triblock copolymers. Formation of a helical morphology in polystyrene-block-polybutadiene-block-poly(methyl methacrylate) block copolymers. *Macromolecules* **28,** 4558–4561 (1995).
22. Auschra, C. & Stadler, R. Synthesis of block copolymers with poly(methyl methacrylate): P(B-b-MMA), P(EB-b-MMA), P(S-b-B-b-MMA). *Polym. Bull.* **30,** 257–264 (1993).

Acknowledgements. V.A. and L.L. thank C. Gay for discussions. L.L. thanks J. Prost and A. Halperin for discussions on longitudinal ferroelectric smectics. This work was supported by INTAS-RFBR, the Deutsche Forschungsgemeinschaft (DFG) and the Bayreuther Institut für Makromolekülforschung (BIMF).

Correspondence and requests for materials should be addressed to V.A. (e-mail: abetz@akstadler.che.uni-bayreuth.de).

Unblocking of the Nares Strait by Greenland and Ellesmere ice-sheet retreat 10,000 years ago

Marek Zreda*, John England†, Fred Phillips‡, David Elmore§ & Pankaj Sharma§

* *Department of Hydrology and Water Resources, University of Arizona, Tucson, Arizona 85721, USA*

† *Department of Earth and Atmospheric Sciences, University of Alberta, Edmonton, Alberta, T6G 2E3, Canada*

‡ *Department of Earth and Environmental Science, New Mexico Tech, Socorro, New Mexico 87801, USA*

§ *Department of Physics, Purdue University, West Lafayette, Indiana 47907, USA*

The extent of glaciation at the northern margin of the Canadian/Greenland high-latitude Arctic region over the past 30,000 years is uncertain. Geological arguments have been made for Greenland and Ellesmere Island ice sheets that coalesced to block the Nares Strait[1], and for restricted ice sheets on the two islands[2] leaving the strait open, as it is today[3]. Distinguishing between these two possibilities would provide significant constraints on present understanding of the past circulation between the Arctic and Atlantic oceans[4,5], on estimates of past ice-volume[6], and on the response of the Greenland ice sheet to climate change[7]. Radiocarbon analyses provide dates for the deglaciation of the islands' coasts, but do not yield information on whether ice filled the strait. Here we present measurements of cosmogenic ^{36}Cl that has accumulated *in situ* in erratics and glacially polished bedrock on islands within the Nares Strait. These data allow us to determine the time for which the rocks have been recently exposed to the atmosphere, and thus the age of the final deglaciation of the strait. We show that Greenland and Ellesmere ice sheets retreated from the Nares Strait about 10,000 years ago. The strait was filled with ice during the last glaciation, blocking this connection between the Arctic and Atlantic oceans, and supporting the model of extensive and long-lasting ice on land and sea in this region[8–11].

The Nares Strait, a body of water 500 km long and 20–100 km wide between Greenland and Ellesmere Island (Fig. 1), has no permanent ice cover and together with other arctic channels carries at present an estimated 30% of the total flow from the Arctic Ocean to the Atlantic Ocean[12]. But in the past, expanded ice sheets filled the strait and drained northward to the Arctic Ocean and southward to Baffin Bay[13]. In the north, Greenland erratics and striated bedrock on Ellesmere[14] and Hans islands[15] record the extent, and northward movement, of the Greenland ice sheet. In the south, erratics and abraded bedrock on both sides of Smith Sound, including Pim Island, indicate southward flow of the coalescent Greenland and Ellesmere ice[10,16,17]. Although the field evidence for the occupation of the Nares Strait by glaciers is unequivocal, the time when it was last glaciated has remained uncertain. If the Nares Strait was last glaciated before Late Wisconsinan times, then a scenario of Late Wisconsinan individual ice caps (the Franklin ice complex)[2] separated by a full-glacial sea[3] would be supported. In this scenario, the northern margin of the Laurentide ice sheet is restricted, and the northwestern margin of the Greenland ice sheet is close to its present position. However, a Late Wisconsinan age for the glacial features would support the existence of the Innuitian ice sheet[1] that coalesced with the Laurentide ice sheet in the south and with the Greenland ice sheet in the northeast. These two scenarios provide entirely different palaeoclimatic interpretations of the ocean circulation during full-glacial times, the response of the Greenland ice sheet to full-glacial climate[7], the flow patterns and thickness of past ice sheets[6,7,18], and the nature of the full-glacial climate in the high-latitude Arctic.

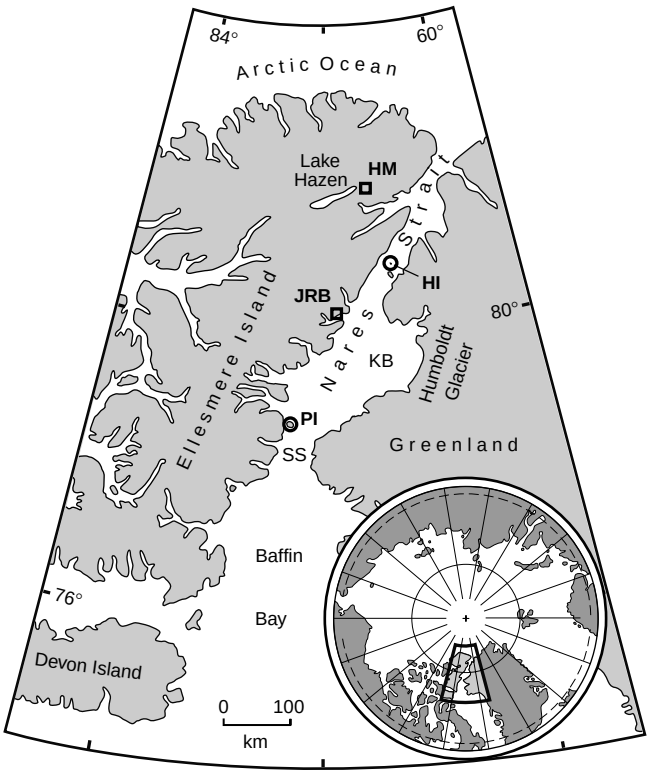

Figure 1 Location of samples for cosmogenic ^{36}Cl dating of late-glacial landforms in the Nares Strait area. Squares, sites used for comparison of ^{36}Cl and ^{14}C ages; circles, sites used for dating of deglaciation of the Nares Strait. Abbreviations of geographical names used in text: HM, Hazen moraines; JRB, John Richardson Bay; HI, Hans Island; PI, Pim Island; KB, Kane basin; SS, Smith Sound. Glacial striations on islands within Nares Strait indicate that ice flow was parallel to the strait, northward on Hans Island and southward on Pim Island. These directions of flow imply a significant thickness of combined Greenland and Ellesmere Island ice, with an ice divide over Kane basin.

We used the cosmogenic ^{36}Cl method[19] to determine surface exposure ages of erratics and bedrock on Hans and Pim islands within the Nares Strait. If the Nares Strait was ice-free since long before the Last Glacial Maximum, bedrock and erratics on islands in the strait would yield cosmogenic exposure ages >35,000 yr. Conversely, if Nares Strait was occupied by ice during the Last Glacial Maximum, cosmogenic ^{36}Cl ages would be <15,000 yr.

To demonstrate the applicability of the cosmogenic ^{36}Cl method in the Arctic and the validity of the production rates determined by our group elsewhere[20], we measured ^{36}Cl in rocks from early Holocene landforms: the Hazen moraines on Hazen plateau and an ice-contact delta in John Richardson Bay (Fig. 1 and Table 1). The moraines are well preserved, with sharp crests, steep slopes and numerous boulders. They extend to raised marine deposits dating between 8,130 and 6,995 ^{14}C yr (refs 3, 21), equivalent to 9,100–7,800 calendar years (cal. yr; correction after Taylor *et al.*[22]). In John Richardson Bay, limestone bedrock littered with abundant boulders was exposed by the retreating ice margin. Marine shells associated with the adjacent ice-contact delta gave a ^{14}C age of 8,050 yr (ref. 23), or ~9,000 cal. yr. Average cosmogenic ^{36}Cl ages for the two features (Table 1 and Fig. 2) agree at the 1σ level with the ^{14}C age estimates. These results show that the ^{36}Cl method yields accurate ages in this region. They also indicate that if individual sample ages show low variability (that is, there are no obvious outliers), the best age estimate is the sample average.

To determine when ice sheets last occupied the Nares Strait, we collected samples of erratics and glacially polished bedrock from two islands in the strait (Fig. 1 and Table 1). On Hans Island, glacially sculpted, striated and plucked limestone bedrock indicates that ice flowed northward[15] from the inferred ice divide in Kane basin[13]. Granite erratics on the bedrock were transported to this site from the interior of Greenland by the precursor of Humboldt Glacier (Fig. 1). On Pim Island, ubiquitous striations and streamlined bedforms were formed on red granitic bedrock by the southward-flowing Smith Sound ice stream[16]. This ice deposited a veneer of till that includes limestone and sandstone erratics from the Proterozoic and Palaeozoic terranes to the north, as well as local granitic boulders.

All but two ^{36}Cl surface exposure ages postdate the Last Glacial Maximum (Table 1 and Fig. 2). On Hans Island, the mean age is

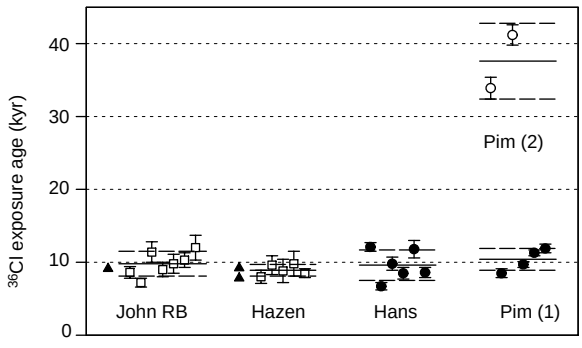

Figure 2 Cosmogenic ^{36}Cl exposure ages of samples from four locations in the Nares Strait area. Black triangles, ^{14}C ages (in calendar years) that we used to validate the ^{36}Cl method. Thick horizontal lines, average surface ages calculated assuming zero erosion; dashed lines above and below represent one standard deviation. Two Pim Island samples have exposure ages that differ from the others by more than five standard deviations. Because these older ages are probably due to ^{36}Cl inherited from previous exposure episodes, we removed them from further consideration. The remaining cosmogenic ^{36}Cl ages from Hans and Pim islands agree numerically with ^{14}C ages of about 9,000–10,000 calendar years for late glacial deposits from both coasts of the Nares Strait.

9,600 ± 2,100 yr and the maximum is 12,100 yr. Individual sample ages have a distribution similar to that for the test samples from John Richardson Bay. There is no systematic difference between lithologies, or between erratics and bedrock, and there is little chance of soil erosion (boulder uncovering) that could affect the age distribution. We therefore consider the average age to be the best estimate for the deglaciation of Hans Island. In contrast, samples from Pim Island fall into two groups with mean ages more than five standard deviations apart. Four younger samples (Pim 1 in Table 1; three erratics and one bedrock) have a mean age of 10,400 ± 1,500 yr and a maximum age of 11,900 yr. Two other samples (Pim 2) have a mean age of 37,600 ± 5,200 yr. This latter age can best be explained by ^{36}Cl inherited from previous exposure to cosmic radiation. Both old samples are from the stoss (up-ice) sides of the summits of two roches moutonnées (protruding hillocks of bedrock), whereas the young bedrock sample is from the plucked lee side of another roche moutonnée. Briner and Swanson[24] have shown that erosion on the stoss side of glacially smoothed bedrock may be insufficient to remove previously accumulated cosmogenic nuclides, while erosion on the lee sides, subject to glacial plucking, is capable of removing inherited nuclides. We observe the same pattern for the bedrock samples from Pim Island. Hence, we consider the younger mean age (10,400 yr) to be our best estimate for the final deglaciation of the island.

Our ^{36}Cl ages demonstrate the coalescent Greenland and Ellesmere Island ice retreated from the Nares Strait about 10,000 yr ago. The ^{36}Cl ages are consistent with ^{14}C ages of 8,000 yr (8,800 cal. yr) for late-glacial deposits on the Greenland coast of the Nares Strait[25] and 9,000 yr (10,000 cal. yr) on the Ellesmere side[10], and with the recent reconstruction of trunk ice retreat from Nares Strait based on ^{14}C-dated glaciomarine deposits[26]. But qualitatively these two types of deglaciation records—one based on ^{14}C, the other on ^{36}Cl—are fundamentally different, and have different palaeoenvironmental implications. The ^{14}C-dated samples indicate when the coastal areas became deglaciated, but do not give information about how far into the strait the former ice extended. The ice could have filled the entire strait, or it could have stopped on the coasts leaving the open sea between Greenland and Ellesmere Island. In both cases, the coastal ^{14}C records would be similar. In contrast, the *in situ* ^{36}Cl data show unequivocally that the Nares Strait was filled with ice until ~10,000 yr ago.

Maximum limiting age estimates for the beginning of the last glacial advance have been obtained from ^{14}C-dated, old marine shells redeposited in till and outwash on the east coast of Ellesmere Island. These ages range from ~30,000 ^{14}C yr (ref. 16) (~36,000 cal. yr; ref. 22) on Cape Herschel, directly west of Pim Island, to 19,000–25,000 ^{14}C yr (~23,000–30,000 cal. yr) farther north and west[26]. Taken together, the youngest of the old ^{14}C ages and our young ^{36}Cl ages constrain the age of the last glaciation of the Nares Strait to have been between 23,000 and 10,000 cal. yr ago. During that period of full-glacial conditions, the connection between the Arctic and the Atlantic oceans via the Nares Strait was closed. This result demonstrates expansion of the Greenland ice sheet during the last glacial period, confirms the filling of the seaways in the high-latitude Arctic by ice during that time, and supports the model of the Innuitian ice sheet bridging the Laurentide and Greenland ice sheets. □

Table 1 ^{36}Cl age determinations and chemical compositions

Sample	Material	^{36}Cl/Cl (10^{-15})	Cl (p.p.m.)	B (p.p.m.)	Gd (p.p.m.)	U (p.p.m.)	Th (p.p.m.)	SiO_2 (wt%)	TiO_2 (wt%)	Al_2O_3 (wt%)	Fe_2O_3 (wt%)	MgO (wt%)	CaO (wt%)	MnO (wt%)	Na_2O (wt%)	K_2O (wt%)	P_2O_5 (wt%)	^{36}Cl age (kyr) $e = 0$	^{36}Cl age (kyr) $e = 5$
Delta. John Richardson Bay, 80.208° N, 71.020° W, 88 m.a.s.l., 8,050 ± 90 ^{14}C yr (ref. 23) = 9,100 cal. yr																			
EI92-20	EL_1.0	112 ± 11	274	25.5	2.5	0.6	1.4	4.96	0.03	1.20	0.27	1.26	50.6	0.01	0.01	0.87	0.07	8.6	8.6
EI92-21	EL_1.0	120 ± 10	132	18.0	0.5	0.5	0.5	2.30	0.01	0.64	0.35	3.58	51.4	0.01	0.01	0.29	0.03	7.2	7.2
EI92-22	EQ_1.0	58 ± 7	64	10.5	0.5	0.5	1.5	93.7	0.04	1.95	0.42	0.09	0.01	0.01	0.01	1.35	0.02	11.4	9.8
EI92-23	EL_0.8	111 ± 13	137	20.5	1.0	0.9	5.2	35.4	0.16	4.58	0.79	2.40	29.8	0.01	0.01	3.47	0.10	9.0	9.0
EI92-24	BL_	201 ± 25	106	26.5	1.0	0.7	1.7	9.94	0.08	2.44	0.90	1.60	47.3	0.01	0.01	0.82	0.07	9.8	9.9
EI92-25	BL_	215 ± 21	95	17.0	1.5	0.6	1.0	10.6	0.04	1.48	0.57	1.40	48.7	0.01	0.01	0.72	0.05	10.3	10.4
EI92-26	EQ_0.6	66 ± 9	29	3.5	0.5	0.5	1.7	97.3	0.06	0.53	0.07	0.06	0.01	0.01	0.01	0.32	0.02	12.0	9.6
Average																		**9.8 ± 1.7**	9.2 ± 1.1
Moraine. Hazen moraine, Hazen plateau, 81.867° N, 68.583° W, 510 m.a.s.l., 8,130 ± 200–6,995 ± 130 ^{14}C yr (refs 3, 21) = 9,200–7,800 cal. yr																			
EI93-46	ES_0.2	148 ± 16	41	(7)	(1)	1.1	5.3	74.4	0.28	5.25	1.67	1.28	8.09	0.03	0.66	1.13	0.10	8.0	7.8
EI93-47	ES_0.5	181 ± 24	35	(7)	(1)	1.2	5.6	71.6	0.37	5.87	2.95	2.62	6.43	0.03	0.34	1.30	0.12	9.6	9.4
EI93-48	ES_0.4	230 ± 42	37	(7)	(1)	1.2	5.6	62.1	0.36	6.83	2.61	2.22	11.8	0.04	0.84	1.59	0.11	8.8	8.8
EI93-49	ES_0.3	184 ± 32	34	7.0	0.5	1.0	3.7	76.1	0.26	5.00	1.91	1.61	6.53	0.03	0.89	1.09	0.08	9.8	9.5
EI93-30	ES_0.7	182 ± 14	44	(7)	(1)	3.0	10.0	64.7	0.52	7.55	2.83	3.10	8.68	0.04	1.30	1.63	0.14	8.5	8.3
Average																		**8.9 ± 0.8**	8.8 ± 0.7
Bedrock and erratics. Hans Island, 80.833° N, 66.583° W, ~150 m.a.s.l.																			
EI92-50	BLP	1015 ± 46	25	8	2	–	–	0.24	0.00	0.01	0.01	0.37	56.00	0.01	0.01	0.15	0.01	12.1	12.6
EI92-61	EGP 0.8	76 ± 6	30	(15)	(5)	0.5	7.6	70.6	0.76	12.8	7.06	2.00	0.74	0.08	1.33	2.55	0.06	6.7	6.7
EI92-52	EG_0.4	75 ± 7	141	85	4	2	12	74.2	0.21	13.4	1.25	30	0.70	0.03	3.91	4.63	0.07	9.8	9.1
EI92-53	BLP	416 ± 39	44	(15)	(5)	0.5	0.5	0.36	0.00	0.06	0.19	0.80	56.20	0.01	0.01	0.04	0.01	8.5	8.7
EI92-54	EG_1.0	77 ± 8	143	2	0.5	0.8	3.6	74.1	0.13	14.0	1.10	0.29	0.89	0.03	4.20	4.51	0.08	11.8	10.6
EI92-55	EL_1.2	610 ± 60	29	(15)	(5)	0.5	0.5	0.27	0.00	0.23	0.06	0.97	55.80	0.01	0.01	0.10	0.02	8.6	8.9
Average																		**9.6 ± 2.1**	9.4 ± 2.0
Bedrock and erratics. Pim Island, 78.708° N, 74.250° W (within 1-km radius), elevations 320, 400, 410, 360, 320, 400 m.a.s.l.																			
EI96-71	EL_1.0	59.4 ± 4.5	577	13.5	2.0	0.7	0.5	4.11	0	0.62	1.63	19.7	28.90	0.08	0.02	0.37	0.01	8.5	7.9
EI96-73	ED_0.4	138 ± 6	29	(15)	(3)	0.5	3.2	67.0	0.55	16.4	4.08	1.63	4.51	0.04	4.76	0.99	0.01	9.7	9.5
EI96-74	EG_ _ _	184 ± 7	24	(15)	(3)	0.5	3.2	70.3	0.35	16.0	2.83	0.62	3.65	0.03	4.83	1.31	0.01	11.3	11.1
EI96-75	BGP	134 ± 7	68	20.5	2.5	0.8	3.3	75.6	0.08	13.7	0.94	0.03	0.71	0.01	3.53	5.07	0.09	11.9	11.6
Average (Pim 1)																		**10.4 ± 1.5**	10.0 ± 1.7
EI96-70	BGS	347 ± 15	74	14.5	3.5	0.9	11.0	73.8	0.15	14.2	1.19	0.15	1.31	0.01	3.60	4.97	0.07	33.9	32.5
EI96-72	BGS	331 ± 11	101	12.0	3.5	1.9	19.0	74.4	0.18	13.9	1.76	0.26	1.26	0.01	3.57	4.45	0.06	41.2	37.4
Average (Pim 2)																		**37.6 ± 5.2**	35.0 ± 3.5

Nomenclature for samples analysed: first letter–Erratic, Bedrock; second letter–Limestone, Quartzite, Sandstone, Granite, Diorite, third letter–glacial Polish or Striae where present; numerical value for erratics–boulder height. For B and Gd, values in brackets indicate estimated concentrations used in the age calculations. Sample ages are calculated using erosion rates (e) of rock surfaces of 0 and 5 mm kyr^{-1}; for these erosion rates, two average surface ages are reported. Individual ages for $e = 5$ are younger than those for $e = 0$ for samples in which neutron activation of ^{35}Cl is an important mechanism of ^{36}Cl formation, and older for samples in which spallation of ^{39}K and ^{40}Ca dominates. Error of surface age is the larger of the internal (analytical uncertainty) and external (natural variability among samples) errors. Numbers in bold-face are our best estimates of surface ages; only these ages are discussed in text.

Methods

Sample preparation. Rock samples were collected from top horizontal surfaces of boulders and bedrock using hammer and chisel. The samples were cleaned of any organic material and carbonate crusts, crushed in a jaw crusher, and ground using a roller grinder. Size fraction 0.25–1.00 mm was leached in 3% nitric acid, rinsed in deionized water, and dried overnight at 100 °C. Silicates were dissolved in a hot mixture of hydrofluoric and nitric acids, carbonates were dissolved in cold diluted nitric acid, and Cl precipitated as AgCl. The AgCl was dissolved in concentrated NH_4OH. Sulphur was precipitated as $BaSO_4$ and separated from the liquid by centrifugation. The liquid was transferred and acidified using HNO_3 to re-precipitate AgCl. The purification step was repeated three times to minimize the amount of sulphur in the final AgCl. Chlorine-36 was determined on AgCl targets by accelerator mass spectrometry (AMS) at PRIME Laboratory, Purdue University. Aliquots of rocks were powdered and analysed for major elements by X-ray fluorescence spectrometry, for U and Th by neutron activation analysis, for B and Gd by neutron activation prompt gamma analysis (all at XRAL Laboratories, Don Mills, Ontario, Canada), and for Cl by an ion-specific electrode.

Age determination. Cosmogenic ^{36}Cl surface exposure ages were calculated using CHLOE software[27], with spallation production rates of 73.3 ± 4.9 atoms ^{36}Cl per g Ca yr^{-1} and 154 ± 10 atoms ^{36}Cl per g K yr^{-1} (ref. 20), and thermal neutron activation production rate calculated[28] from the fast neutron production rate of 586 ± 40 neutrons per g air yr^{-1} (ref. 20). We used these production rates because: (1) they have been determined using a large number of samples of different ages and from 15 separate surfaces at eight locations (other production rates include fewer samples from fewer localities); (2) production rates from all three target elements (Cl, K and Ca) have been calculated simultaneously (other production rates have been determined for one or two elements); and (3) field and laboratory procedures used in the production-rate study and in this research were identical, which assures compatibility of all samples. Should the production rates change, the exposure ages can be recalculated using Table 1, which contains all the necessary data. The production rates used here are for sea level and high latitudes, and were scaled[29] to the locations of sample sites. It was not necessary to correct the production rates for temporal variability because at high latitudes the cosmic-ray intensity is constant. Likewise, the correction for seasonal snow cover is minimal in this relatively dry environment (precipitation rate, 50–100 mm yr^{-1}). All samples were collected above the Holocene marine limit (110–120 m), which means that they have been above sea level since deglaciation; therefore, no correction for water shielding was needed. Uncertainties of the ^{36}Cl ages (a combination of analytical errors and systematic errors associated with production-rate calculations) have been estimated to be $<15\%$ for studies in which multiple samples were analysed[30].

Received 31 March; accepted 22 December 1998.

1. Blake, W. Jr Studies of glacial history in Arctic Canada. I. Pumice, radiocarbon dates and differential post-glacial uplift in the eastern Queen Elizabeth Islands. *Can. J. Earth Sci.* **7,** 634–664 (1970).
2. England, J. Late Quaternary glaciation of the northeastern Queen Elizabeth Islands, N.W.T., Canada; alternative models. *Quat. Res.* **6,** 185–202 (1976).
3. England, J. Isostatic adjustments in a full glacial sea. *Can. J. Earth Sci.* **20,** 895–917 (1983).
4. Aksu, A. E. & Piper, D. J. W. Baffin Bay in the past 100,000 yr. *Geology* **7,** 245–248 (1979).
5. Aksu, A. E. in *Quaternary Environments: the Eastern Canadian Arctic, Baffin Bay and West Greenland* (ed. Andrews, J. T.) 181–209 (Allen & Unwin, Boston, 1985).
6. Peltier, W. R. Mantle viscosity and ice-age ice sheet topography. *Science* **273,** 1359–1364 (1996).
7. Cuffey, K. M. & Clow, G. D. Temperature, accumulation, and ice sheet elevation in central Greenland through the last deglacial transition. *J. Geophys. Res.* **102,** 26383–26396 (1997).
8. Hughes, T., Denton, G. H. & Grosswald, M. G. Was there a late-Würm arectic ice sheet? *Nature* **266,** 596–602 (1977).
9. Tushingham, A. M. On the extent and thickness of the Innuitian Ice Sheet: a postglacial-adjustment approach. *Can. J. Earth Sci.* **28,** 231–239 (1991).
10. Blake, W. Jr Holocene emergence at Cape Herschel, east-central Ellesmere Island, arctic Canada: implications for ice sheet configuration. *Can. J. Earth Sci.* **29,** 1958–1980 (1992).
11. Funder, S. & Hansen, L. The Greenland ice sheet—a model for its culmination and decay during and after the last glacial maximum. *Bull. Geol. Soc. Denmark* **42,** 137–152 (1996).
12. Aagaard, K. & Carmack, E. C. The role of sea ice and other fresh water in the arctic circulation. *J. Geophys. Res.* **94,** 14485–14498 (1989).
13. Funder, S. in *Quaternary Geology of Canada and Greenland* (ed. Fulton, R. J.) 743–792 (Geological Survey of Canada, Ottawa, 1989).
14. England,, J. Advance of the Greenland Ice Sheet on to north-eastern Ellesmere Island. *Nature* **252,** 373–375 (1974).
15. de Freitas, T. A. Implications of glacial sculpture on Hans Island, between Greenland and Ellesmere Island. *J. Glaciol.* **36,** 129–130 (1990).
16. Blake, W. Jr Shell-bearing till along Smith Sound, Ellesmere Island–Greenland: age and significance. *Sveriges Geologiska Undersökning* **81,** 51–58 (1992).
17. Blake, W. Jr, Boucherle, M. M., Fredskild, B., Janssens, J. A. & Smol, J. P. The geomorphological setting, glacial history and Holocene development of "Kap Inglefield Sø", Inglefield Land, North-West Greenland. *Meddelelser om Grønland* **27,** 1–42 (1992).
18. Reeh, N. Was the Greenland ice sheet thinner in the late Wisconsinan than now? *Nature* **317,** 797–799 (1985).
19. Phillips, F. M., Leavy, B. D., Jannik, N. O., Elmore, D. & Kubik, P. W. The accumulation of cosmogenic chlorine-36: a method for surface exposure dating. *Science* **231,** 41–43 (1986).
20. Phillips, F. M., Zreda, M. G., Flinsch, M. R., Elmore, D. & Sharma, P. A reevaluation of cosmogenic ^{36}Cl production rates in terrestrial rocks. *Geophys. Res. Lett.* **23,** 949–952 (1996).
21. England, J. The glacial geology of northeastern Ellesmere Island, Northwest Territories, Canada. *Can. J. Earth Sci.* **15,** 603–617 (1978).
22. Taylor, R. E., Stuiver, M. & Reimer, P. J. Development and extension of the calibration of the radiocarbon time scale: archeological applications. *Quat. Sci. Rev.* **15,** 655–668 (1996).
23. England, J. Glacier dynamics and paleoclimatic change during the last glaciation of eastern Ellesmere Island, Canada. *Can. J. Earth Sci.* **33,** 779–799 (1996).
24. Briner, J. P. & Swanson, T. W. Using inherited cosmogenic ^{36}Cl to constrain glacial erosion rates of the Cordilleran ice sheet. *Geology* **26,** 3–6 (1998).
25. Kelly, M. & Bennike, O. *Quaternary Geology of Western and Central North Greenland* (Geological Survey of Greenland, Copenhagen, 1992).
26. England, J. Support for the Innuitian Ice Sheet in the Canadian High Arctic during the Last Glacial Maximum. *J. Quat. Sci.* **13,** 275–280 (1998).
27. Phillips, F. M. & Plummer, M. A. CHLOE: A program for interpreting *in-situ* cosmogenic nuclide data for surface exposure dating and erosion studies. (abstr.) *Radiocarbon* **38,** 98 (1996).
28. Liu, B., Phillips, F. M., Fabryka-Martin, J. T., Fowler, M. M. & Biddle, R. S. Cosmogenic ^{36}Cl accumulation in unstable landforms, 1, Effects of the thermal neutron distribution. *Wat. Resour. Res.* **30,** 3115–3125 (1994).
29. Lal, D. Cosmic ray labeling of erosion surfaces: *in situ* nuclide production rates and erosion models. *Earth Planet. Sci. Lett.* **104,** 424–439 (1991).
30. Phillips, F. M. *et al.* Cosmogenic ^{36}Cl and ^{10}Be ages of Quaternary glacial and fluvial deposits of the Wind River Range, Wyoming. *Geol. Soc. Am. Bull.* **109,** 1453–1463 (1997).

Acknowledgements. This work was supported by the NSF, through grants from the Geosciences Directorate (to F.M.P.) and the Office of Polar Programs (to M.Z.), and by the David and Lucile Packard Foundation, through the Fellowship in Science and Engineering (to M.Z.). AMS work was supported by the NSF (grants to D.E.). Field work was organized by J.E. and supported by the Polar Continental Shelf Project (Natural Resources Canada).

Correspondence and requests for materials should be addressed to M.Z. (e-mail: marek@hwr.arizona.edu).

The role of hydraulic fractures and intermediate-depth earthquakes in generating subduction-zone magmatism

J. Huw Davies

Department of Earth Sciences, The University of Liverpool, Liverpool L69 3BX, UK

The presence of magmatism and intermediate-depth (70–300 km deep) seismicity at subduction zones is at first sight surprising. Magmatism is unexpected because the subduction of cool oceanic lithosphere makes these regions the coldest in the mantle. The current model for subduction-zone magmatism is that water released from the subducting slab enters the relatively warm mantle wedge, leading to a reduction in melting temperature and magmatism[1–4]. But there is a problem with this scheme because it is thought that water cannot leave the slab by porous flow to enter the wedge. The occurrence of intermediate-depth earthquakes is surprising because of the inhibitory effect of the very high frictional stress on faults expected from the high pressure at these depths. One proposal put forward to explain intermediate-depth seismicity is that high pore-pressure might facilitate faulting by decreasing the friction[5–7]. The hypothesis presented here is that non-percolating water provides the high pore-pressure, that the consequent faulting temporarily interconnects the water pores and, when a sufficient vertical height of water is interconnected, a hydrofracture is produced which transports the water out into the mantle wedge, thereby generating subduction-zone magmatism.

Hydrous minerals are formed in oceanic crust by hydrothermal circulation at mid-ocean ridges. This water is then released in subducting slabs by dehydration reactions due to increasing temperature and pressure encountered during subduction. A lateral transport mechanism has been proposed for moving water horizontally across the mantle away from the cold slab out to the hot mantle wedge. The water reacts with mantle peridotite forming